Charged particle induced etching and functionalization of two-dimensional materials.

Journal:	*ECS Journal of Solid State Science and Technology*
Manuscript ID	Draft
Manuscript Type:	Research Paper
Date Submitted by the Author:	n/a
Complete List of Authors:	Elbadawi, Christopher; University of Technology Sydney - City Campus, Mathematical and Physical Sciences Kianinia, Mehran; University of Technology Sydney - City Campus, Mathematical and Physical Sciences Bendavid, Avi; CSIRO Lobo, Charlene; University of Technology Sydney - City Campus, Mathematical and Physical Sciences; University of Technology Sydney - City Campus,
Keywords:	electron beam induced etching, hexagonal boron nitride, black phosphorus, charged particle, environmental scanning electron microscopy

Charged particle induced etching and functionalization of two-dimensional materials

Christopher Elbadawi[1], Mehran Kianinia[1], Avi Bendavid[2], and Charlene J. Lobo[1z],

[1]School of mathematical and physical sciences, University of Technology Sydney, Sydney NSW 2007 Australia.
[2]CSIRO Manufacturing, Lindfield NSW 2070 Australia.

[z]Corresponding Author E-mail Address [charlene.lobo@uts.edu.au]

Abstract Text

Focused electron beam induced deposition and etching (FEBID and FEBIE) are direct-write nanofabrication techniques in which an electron beam is used to achieve nanostructure functionalization, etching or deposition. Either alone or in combination with *in situ* plasmas, these techniques can also be used to accelerate reactions that occur in ambient environment, with simultaneous high-resolution imaging. Here, we describe our recent work on etching, functionalization and directed assembly of a range of nano- and two-dimensional materials using temperature-dependent FEBIE experiments in an environmental scanning electron microscope (ESEM). As examples of the application of these techniques, we demonstrate processes for assembling arrays of nanodiamonds that can be used as magnetic field sensors, as well as for controlled etching of hexagonal boron nitride (hBN) and black phosphorus (BP).

Introduction

Chemical functionalization of two-dimensional and nanoscale materials is of interest for applications in sensing, photocatalysis and electrochemistry, and energy storage. Functionalization of graphene, transition metal dichalcogenides and the MXenes, diamond and hBN, generally requires high temperatures and/or the use of highly energetic processes such as electrochemistry, electron/ion beam irradiation or thermal activation[1]. However, many 2D materials are at the other end of the reactivity scale, such as the elemental two-dimensional (2D) semiconductors black phosphorus (BP), germanene and silicene. Despite having electronic properties that rival silicon and graphene, these 2D semiconductors are highly unstable in ambient and aqueous environments. Black phosphorus also has greater biocompatibility, higher surface-to-volume ratio, higher molecular adsorption energies and lower out-of-plane electrical conductance than graphene and transition metal dichalcogenides, making it highly advantageous in applications such as energy storage[2], neuromorphic and biomedical devices[3], field effect transistors[4] and photodetectors[5].

There are very few techniques that permit real-time imaging and/or spectroscopy of the reaction chemistry of these emerging materials at the required nanometre resolution, with existing methods including environmental scanning and transmission electron microscopy[6], scanning near-field optical microscopy[7], and scanning electrochemical microscopy[8]. One of the most promising methods is electron beam induced chemistry in an ESEM[9]. In this paper, which was recently presented at IUMRS-ICA 2021 in Jeju, Korea, we discuss the

development of successful strategies employing charged particle beams for assembly, functionalization and etching of two-dimensional and nanoscale semiconductors such as nanodiamonds, hBN and BP.

ESEM can be used to accelerate reactions that occur in ambient environment while allowing simultaneous high-resolution imaging. Prior studies have shown that localized low-energy electron beam chemistry enables sculpting, etching and fabrication of devices at nanoscale resolution without causing larger-scale damage. For example, etching of diamond using a low energy (1-2 keV) electron beam in a low vacuum H_2O environment enables the fabrication of high aspect ratio, micron-scale diamond antennas that enhance the 630 nm emission from embedded nitrogen vacancy centre[10]. The technique has also been used for nanoscale deposition of magnetic tips on scanning probes[11]. The mechanistics of charged particle induced etch, deposition and nanofabrication processes have also been studied in detail[12–15] and are reviewed in Ref. [16].

Experimental methods

Substrate and sample preparation

Nanoscale and two-dimensional materials (nanodiamonds, hBN, or mechanically exfoliated BP flakes) were deposited onto a plasma-cleaned thermally oxidized silicon substrate. Prior to loading in the ESEM chamber, the few-layer BP samples were kept in pristine condition by shielding from light and storing them in a low vacuum desiccator. Nanodiamond and hBN samples were stored in ambient conditions prior to ESEM experiments.

Samples were then loaded into the ESEM chamber, which was pumped down to the base pressure of 3×10^{-4} Pa. Prior to ESEM experiments, nanodiamonds and hBN samples were cleaned of carbon contaminants using an *in situ* delocalized plasma treatment (15 W in a low-vacuum O_2 environment) overnight at room temperature. The plasma treatment improves EBIE repeatability and enables quantitative measurements of etch rates, without causing etching or damage to the sample.

RIE plasma treatment

An inductively coupled reactive ion etching (RIE) plasma operating at 100 W and 6 Pa NH_3 was used for amine-functionalization experiments. These conditions have been previously reported to produce a high concentration of NH_2 groups in the plasma[17].

X-ray photoelectron spectroscopy (XPS)

XPS was used to establish the effectiveness of the plasma process for amination of the carbon seeds used for directed assembly of nanodiamonds. The chemical bonding of the surfaces was assessed by using a Specs 150 SAGE instrument operated with a Mg Kα X-ray source (Mg anode operated at 10 keV and 10 mA). The C1s peak at 284.6 eV was used as a reference to

compensate for any surface charging.

ESEM experiments

All ESEM experiments were conducted using a variable pressure FEI Sirion scanning electron microscope. For experiments using gases other than water, a cold trap was employed to minimise the effect of residual H_2O. Each sample was held at the chosen temperature (25ºC -150ºC) and imaged during electron irradiation using a magnetic-field-assisted helix gaseous secondary electron detector. Further details of the experimental setup and methodology are provided in Refs. [18–21]

Confocal PL spectroscopy

Confocal PL measurements were done at room temperature using a high numerical aperture objective (100X, 0.9 N.A) for both excitation and collection of the emitted light, and a 532 nm continuous wave laser for excitation.

Results and discussion

Beam-directed assembly of nanodiamonds

Nanodiamonds are widely employed as hosts of optically-active defects such as the NV^- centre, which is of high interest in photonics and quantum control applications due to its triplet ground state. This results in a zero-field magnetic resonance at 2.88 GHz and a bright zero phonon emission line at 637 nm. Due to this rather unique combination of properties, the NV^- centre has become a widely studied defect with applications in quantum information[22] and memories[23], sensing[24] and magnetic resonance imaging technologies[25]. NV^- centres can be created by high-energy irradiation processes or during nanodiamond growth. The latter method produces higher quality defects than irradiation without requiring post-processing such as high temperature annealing. However, the deterministic creation of NV- defects in diamond is extremely challenging, as is accurate positioning of single NV^- centres for devices utilizing the centre's unique single photon emission and magnetic resonance properties.

We have pioneered the use of focused electron beam irradiation with nanoscale resolution to achieve highly localized directed assembly of nanodiamonds at previously-defined locations. In order to achieve this, we developed a multi-step process that is illustrated in Figure 1a. In the first step, an array of carbon seeds was deposited on an oxidized and plasma cleaned silicon substrate by focused electron beam deposition from a naphthalene ($C_{10}H_8$) precursor (Fig. 1b). In the second step, the carbon seed array was exposed to an NH_3 plasma for 30 seconds, along with a reference carbon film deposited by electron beam evaporation. XPS measurements were then performed on a clean SiO_2/Si substrate and the carbon-coated film (Fig 2a), as the carbon seeds did not cover a sufficient proportion of the substrate to permit collection of high quality XPS data. The XPS data from the plasma-treated carbon film demonstrates that this procedure is highly selective, resulting in amine functionalization only of the carbon film (Fig. 2b), while the surrounding SiO_2/Si surface remains oxygen-terminated. In addition, N1s XPS spectra taken after plasma

treatment reveals that the ammonia plasma treated carbon contains both amine and amide groups (Fig 2c), both of which are suitable for coupling to carboxyl groups on the nanodiamond surface using carbodiimide conjugation. Unlike the C-F peak in Fig. 2a and 2b, which is present both before and after plasma treatment and likely results from chamber contamination, the N1s peak was not detected prior to plasma treatment.

In the final step of nanodiamond assembly, the aminated carbon seeds are functionalized with 1-ethyl-3(3-dimethylaminopropyl)carbodiimide (EDC). EDC is a linker molecule that binds the carboxylic acid (-COOH) groups on the nanodiamond surfaces to the amine-terminated carbon seeds via carbodiimide coupling chemistry (Fig. 1a). The full conjugation and assembly process is described in Ref.[21].

The result is shown in the confocal PL image of the nanodiamond-carbon seed array (Fig. 3a and 3b), in which the bright dots are the 637 nm zero-photon PL emission from the NV^- centres in the nanodiamonds (Fig. 3d). Statistical analysis of the array (Fig. 3c) shows that NV^- centres are bound to 32 out of 35 seeds in the array (a 92% attachment yield). There are no nanodiamonds bound to positions in between the carbon seeds, showing that this assembly method is highly specific to the amine-functionalized carbon rather than the oxygen-terminated SiO_2 substrate. Variations in the PL intensity from each seed in the array are due to differences in the number of NV^- centres within each nanodiamond, as well as differences in the number of nanodiamonds bound to each seed. Very recently, other researchers have also demonstrated direct printing of nanodiamonds via electrohydrodynamic printing, which is higher throughput but suffers from much lower resolution than electron beam deposition[26].

Dynamic imaging of charged particle induced reactions

In addition to directed self-assembly of nanoparticles, charged particle beams have been used to create optically active defects in a range of materials, including diamond, gallium nitride, and hBN[27,28]. The effect of focused electron beam irradiation can be tuned by appropriate selection of the accumulated electron dose: in hBN for example, low electron doses produce nitrogen vacancy defects emitting single photons[28], while high electron doses controllably etch the material[29]. [30].

The dose-dependence of the charged particle induced reaction process can be exploited to accelerate reactions that occur in ambient environment, as well as to conduct dynamic and mechanistic studies of electron, ion and plasma induced reactions. Here, we will discuss two such studies: H_2O-mediated electron beam etching of hBN, and H_2O-induced degradation of few-layer BP.

Hexagonal boron nitride is a wide-bandgap insulator which is widely used as a dielectric substrate or encapsulating material for graphene and two-dimensional in a wide range of optoelectronic and photonic devices. hBN has exceptionally high thermal and chemical stability, and is resistant to most chemical reaction and diffusion processes including etching by strong acids and high-temperature oxygen diffusion[31]. Oxidative etching of hBN normally requires a high activity metal catalyst such as Ag nanoparticles[32]. However, by using H_2O as the etch precursor in a focused electron beam induced etch (EBIE) process, we have achieved highly controlled nanoscale etching of hBN without any catalyst[29]. Etching of hBN was conducted under a background H_2O pressure of 8 Pa H_2O at 15 or 25 keV accelerating voltage and 1.35 nA beam current. As shown in Fig. 4, the etch process initially causes

roughening of the hBN surface, followed by the formation of nanoparticles with diameters ~ 30 nm, and finally resulting in the complete removal of hBN under the electron beam. Nanoparticles build up on the surface for the first 30 minutes of the etch process (Fig. 4(a)-(c)), but then start to disappear, leaving a clean surface in the electron-beam irradiated region after ~ 60 minutes (Fig. 4 (d)-(f)). Compositional and microstructural analysis of the nanoparticles, roughened and clean surfaces was conducted by energy dispersive spectroscopy (EDS), auger electron spectroscopy (AES) and transmission electron microscopy (TEM)[29], revealing that the nanoparticles are created by fragmentation of the hBN and are composed only of B and N.

The sequence of reactions that take place during the H_2O-mediated EBIE process is believed to be as follows. In the first step, the focused electron beam breaks B-N substrate bonds at the surface to produce BN fragment nanoparticles. Upon further electron beam exposure in H_2O vapour, these BN nanoparticles are volatilized, likely resulting from the production of nitric and boric acids in the beam-irradiated region.

The first step of the volatilization process is adsorption and dissociation of surface adsorbed H_2O to produce adsorbed H* and OH* species:

$$H_2O\ (ads) \rightarrow\ H^*\ (ads) +\ OH^*(ads)$$

Reaction of the surface-adsorbed N*, OH*, and O* species with BN fragments then produces nitric and boric acids in the beam-irradiated region:

$$N^* + OH^* +\ 2O^* \rightarrow\ HNO_3(aq)$$

$$2B^* + 3O^*\ \rightarrow\ B_2O_3(aq)$$

While boric acid is a very weak acid, the nitric acid produced by this process is concentrated enough to locally etch silver nanowires supported on the hBN, as discussed in Ref. [33], and thus concentrated enough to etch away any remaining BN nanoparticles, resulting in the clean SiO_2 substrate shown in Fig 4(f).

Like hBN, few-layer BP can be mechanically exfoliated to produce mono- and multi-layers. However, in contrast to hBN, BP is highly unstable in ambient environment, being rapidly degraded upon exposure to even low percentages of water vapour. This high reactivity and lack of stability poses a problem for fabrication, testing and prototyping of biomedical, sensing and photonic devices using standard techniques such as focused ion beam or reactive plasma irradiation. Even relatively thick (5 nm) Al_2O_3 passivating layers used in optoelectronic device fabrication still permit oxidation and resultant rapid degradation of the underlying BP. The etch reaction of BP in ambient environment has been intensively studied and found to begin with formation of a phosphorous oxide (P_2O_5) surface layer, which is converted to phosphoric acid upon water adsorption or interaction with reactive oxygen species[34–36]. Here, we use ESEM in a low-pressure H_2O environment to study the dynamics of the H_2O-mediated etch process in real-time.

Prior to ESEM experiments, few-layered BP flakes with average thickness of 50 nm were mechanically exfoliated from commercial black phosphorus crystals onto a thermally oxidized silicon substrate. BP samples were kept in pristine condition by shielding them from light and storing them in a low vacuum desiccator to prevent reaction with moisture. The BP was loaded into the ESEM chamber, which was then pumped down to the base pressure of 3 x 10^{-4} Pa. *In situ* electron beam irradiation in a background chamber pressure of 8 Pa H_2O was conducted in ESEM mode at 15keV accelerating voltage and 5.6 nA beam current. Each BP sample was held at the appropriate temperature (25ºC -150ºC) and imaged during electron irradiation using a magnetic-field-assisted helix gaseous secondary electron detector. Further details of the experimental setup and methodology are provided in Ref. [19].

Electron irradiation in 8 Pa H_2O resulted in the formation of P_2O_5 bubbles followed by the reaction of these bubbles with dissociated H_2O, leading to rapid degradation and volatilization of the BP. Prior studies under ambient conditions suggest that the bubbling is caused by dissociative chemisorption of oxygen onto the BP flakes, followed by further reaction with adsorbed H_2O[34,35,37]. Because the ESEM experiment is performed at elevated temperatures (between 25 and 150 ºC), and residual atmospheric gases (such as O_2 and N_2) are removed via a cold trap in the gas line, the only mobile adsorbates in our experiment are believed to be physisorbed H_2O molecules and the aqueous reaction product H_3PO_4. Both electron irradiation and H_2O are necessary for degradation to occur, consistent with previous observations that humidity alone does not cause BP degradation[19,36].

The electron-induced BP degradation reaction can be described by two steps accounting for (1) dissociation of adsorbed H_2O, and (2) reaction of the dissociated OH^- and H^+ species with the P_2O_5 surface oxide to produce phosphoric acid (H_3PO_4):

$$H_2O\,(ads) + e \rightarrow H^+\,(ads) + OH^-(ads) \quad (1)$$

$$P_2O_5(s) + 3H^+\,(ads) + 3OH^-\,(ads) \rightarrow 2H_3PO_4\,(ads) \quad (2)$$

The steps involved in the BP degradation reaction are clearly shown in the video attached as **Supplementary Material**, where defected edge sites created or activated by electron beam irradiation appear as bright spots in the SEM image, and the generated phosphoric acid diffuses from these sites in a propagating reaction front that rapidly leads to complete volatilization of the BP flake. Videos were obtained by rastering the electron beam over a selected region of each BP flake, using a screen capture rate of 2 seconds per screenshot (0.5 frames per s) at an electron beam flux of 4.42x10^{17} electrons $cm^{-2}min^{-1}$. Each video was recorded under 8 Pa H_2O for 90 mins. (Note that the video in the Supplementary Information has been sped up 30 times, ie. 1 second of video equates to 1 min. electron beam irradiation).

As the overall reaction is rate limited by the diffusion of H_2O adsorbates in step (1), it can in principle be modelled as a one-dimensional diffusion equation similar to the CO system discussed in Ref. [38], with the reaction front velocity v being proportional to the square root of the reactant diffusion coefficient(s) D multiplied by a rate limiting constant k. The front velocity at substrate temperatures ranging from RT (25 ºC=298K) to 150 ºC (423 K) was calculated from analysis of video screen captures taken during the reaction at successive timepoints after the onset of degradation at time t_0. ImageJ processing software was then used to measure the distance of the reaction-diffusion front from the origin (centre of the circle in Fig. 5a) at five locations in each screen capture, and the average distance at time t_0 after the degradation onset was converted to a front velocity v. For example, Figure 5 displays a series

of frames captured during the electron beam induced process at room temperature (25 ºC), where t_0=720 s (the full video appears in the **Supplementary Material**).

The time for onset of degradation of the BP decreases exponentially with increasing temperature up to 100 ºC (Fig. 6a), being 12 minutes (720 s) at 25 ºC and just over 2 minutes (120 s) at 100 ºC. The decreasing onset time with increasing temperature results from the increasing rate of surface diffusion of water molecules with increasing temperature (according to $D = D_0 e^{-E_{diff}/kT}$), which increases the rate of production of H^+ and OH^- etch species in equation 1. For water, D_o=1x10^{13} A^2/s^2 and the activation energy for diffusion E_{diff} is estimated at 0.13 eV (ref [39]). Once created, the H^+ and OH^- etch species react with the P_2O_5 surface oxide to produce H_3PO_4 (equation 2). However, the residence times ($\tau = \tau_0 e^{E_{des}/kT}$) of H_2O and H_3PO_4 molecules exhibit a stronger exponential decrease with increasing temperature than the increase in the rate of diffusion, leading to a decrease in the front velocity with increasing temperature (Fig. 6b). At 100ºC, and with τ_o=1x10^{-13} s and E_{des}=0.455 eV, the residence time of H_2O is estimated[15] at 1.4x10^{-7} s, with a similar value for H_3PO_4. Thus, above 100 ºC these molecules do not reside on the BP surface long enough to interact with the electron beam, and the degradation reaction cannot take place.

The overall temperature dependence of BP degradation reveals that the primary role of the electron beam is to activate defect sites (predominantly at the flake edges) where the diffusing H_2O molecules are able to physisorb and then undergo electron induced dissociation to produce reactive H^+ and OH^- species. Because of the relatively weak adsorption, raising the temperature slightly above 100ºC is a simple method of preventing degradation of BP in humid and ambient environments. In contrast, the rate of electron beam induced etching of hBN in H_2O is independent of temperature between 25 and 325 ºC, because chemisorption rather than physisorption of H_2O is necessary for degradation of hBN to occur[29].

Conclusions

In conclusion, this work demonstrates the utility of environmental scanning electron microscopy for nanoparticle assembly, etching of two-dimensional materials, and studying the dynamics of chemical reactions at the surfaces of nanostructured and two-dimensional materials. As examples of the application of these techniques, we demonstrate processes for assembling arrays of nanodiamonds into magnetic sensors, controlled nanoscale etching of hexagonal boron nitride (hBN) in water vapour, and for controlling the degradation of BP in ambient and humid environments.

References

1. Karkas, M. D. Electrochemical strategies for C-H functionalization and C-N bond formation. *Chemical Society Reviews* **47**, 5786–5865 (2018).
2. Jin, H. C. *et al.* Black phosphorus composites with engineered interfaces for high-rate high-capacity lithium storage. *Science* **370**, 192-+ (2020).
3. Luo, M. M., Fan, T. J., Zhou, Y., Zhang, H. & Mei, L. 2D Black Phosphorus-Based Biomedical Applications. *Advanced Functional Materials* **29**, (2019).
4. Kim, S. *et al.* Thickness-controlled black phosphorus tunnel field-effect transistor for low-power switches. *Nature Nanotechnology* **15**, 203-+ (2020).
5. Chen, Y. F. *et al.* Unipolar barrier photodetectors based on van der Waals heterostructures. *Nature Electronics* **4**, 357–363 (2021).
6. Luo, L. L. *et al.* Revealing the reaction mechanisms of Li-O-2 batteries using environmental transmission electron microscopy. *Nature Nanotechnology* **12**, 535-+ (2017).
7. Gamage, S. *et al.* Nanoscopy of Black Phosphorus Degradation. *Advanced Materials & Interfaces* **3**, (2016).
8. Kai, T. H., Zoski, C. G. & Bard, A. J. Scanning electrochemical microscopy at the nanometer level. *Chemical Communications* **54**, 1934–1947 (2018).
9. Toth, M. Advances in gas-mediated electron beam-induced etching and related material processing techniques. *Applied Physics A* **117**, 1623–1629 (2014).
10. Martin, A. A., Toth, M. & Aharonovich, I. Subtractive 3D printing of optically active diamond structures. *Scientific reports* **4**, (2014).
11. Pablo-Navarro, J., Sangiao, S., Magen, C. & de Teresa, J. M. Magnetic Functionalization of Scanning Probes by Focused Electron Beam Induced Deposition Technology. *Magnetochemistry* **7**, (2021).
12. Toth, M., Lobo, C., Friedli, V., Szkudlarek, A. & Utke, I. Continuum models of focused electron beam induced processing. *Beilstein journal of nanotechnology* **6**, 1518–1540 (2015).
13. Bishop, J. *et al.* Role of Activated Chemisorption in Gas-Mediated Electron Beam Induced Deposition. *Phys. Rev. Lett.* **109**, 146103 (2012).
14. Toth, M. *et al.* Nanostructure fabrication by ultra-high-resolution environmental scanning electron microscopy. *Nano Letters* **7**, 525–530 (2007).
15. Toth, M., Lobo, C. J., Hartigan, G. & Ralph Knowles, W. Electron flux controlled switching between electron beam induced etching and deposition. *Journal of Applied Physics* **101**, 54309 (2007).
16. Utke, I., Moshkalev, S. & Russell, P. *Nanofabrication using focused ion and electron beams: principles and applications*. (Oxford University Press, 2012).
17. Steen, M. L., Kull, K. R. & Fisher, E. R. Comparison of surface interactions for NH and NH2 on polymer and metal substrates during NH3 plasma processing. *Journal of applied physics* **92**, 55–63 (2002).
18. Lobo, C. J. *et al.* Gas mediated charged particle beam processing of nanostructured materials. *Laser 3D Manufacturing* vol. 8970 (2014).
19. Elbadawi, C. *et al.* Encapsulation-Free Stabilization of Few-Layer Black Phosphorus. *ACS applied materials & interfaces* **10**, 24327–24331 (2018).
20. Elbadawi, C., Toth, M. & Lobo, C. J. Pure Platinum Nanostructures Grown by Electron Beam Induced Deposition. *ACS applied materials & interfaces* **5**, 9372–9376 (2013).
21. Kianinia, M. *et al.* Robust, directed assembly of fluorescent nanodiamonds. *Nanoscale* **8**, 18032–

18037 (2016).
22. Siyushev, P. *et al.* Photoelectrical imaging and coherent spin-state readout of single nitrogen-vacancy centers in diamond. *Science* **363**, 728-+ (2019).
23. Fuchs, G. D., Burkard, G., Klimov, P. v & Awschalom, D. D. A quantum memory intrinsic to single nitrogen-vacancy centres in diamond. *Nature Physics* **7**, 789–793 (2011).
24. Schirhagl, R., Chang, K., Loretz, M. & Degen, C. L. Nitrogen-Vacancy Centers in Diamond: Nanoscale Sensors for Physics and Biology. in *Annual Review of Physical Chemistry, Vol. 65* (eds. Johnson, M. A. & Martinez, T. J.) vol. 65 83–105 (2014).
25. Mamin, H. J. *et al.* Nanoscale Nuclear Magnetic Resonance with a Nitrogen-Vacancy Spin Sensor. *Science* **339**, 557–560 (2013).
26. Xu, Z. Y. *et al.* On-Demand, Direct Printing of Nanodiamonds at the Quantum Level. *Advanced Science* 2103598 (2021) doi:10.1002/advs.202103598.
27. Choi, S. *et al.* Engineering and localization of quantum emitters in large hexagonal boron nitride layers. *ACS Applied Materials & Interfaces* **8**, 29642–29648 (2016).
28. Tran, T. T. *et al.* Robust multicolor single photon emission from point defects in hexagonal boron nitride. *ACS Nano* **10**, 7331–7338 (2016).
29. Elbadawi, C., HuaáLi, L. & others. Electron beam directed etching of hexagonal boron nitride. *Nanoscale* **8**, 16182–16186 (2016).
30. Froch, J. E. *et al.* Versatile direct-writing of dopants in a solid state host through recoil implantation. *Nature Communications* **11**, (2020).
31. Liu, Z. *et al.* Ultrathin high-temperature oxidation-resistant coatings of hexagonal boron nitride. *Nature Communications* **4**, (2013).
32. Liao, Y. *et al.* Oxidative etching of hexagonal boron nitride toward nanosheets with defined edges and holes. *Scientific Reports* **5**, (2015).
33. Elbadawi, C., Froch, J. E., Aharonovich, I., Toth, M. & Lobo, C. J. One-Step Nanoscale Patterning of Silver Nanowire-Nitride Heterostructures Using Substrate-Assisted Chemical Etching. *Journal of Physical Chemistry C* **123**, 945–949 (2019).
34. Hanlon, D. *et al.* Liquid exfoliation of solvent-stabilized few-layer black phosphorus for applications beyond electronics. *Nature Communications* **6**, (2015).
35. Favron, A. *et al.* Photooxidation and quantum confinement effects in exfoliated black phosphorus. *Nature Materials* **14**, 826 (2015).
36. Walia, S. *et al.* Ambient Protection of Few-Layer Black Phosphorus via Sequestration of Reactive Oxygen Species. *Advanced Materials* (2017).
37. Wang, G., Slough, W. J., Pandey, R. & Karna, S. P. Degradation of phosphorene in air: understanding at atomic level. *2D Materials* **3**, 25011 (2016).
38. Rotermund, H. H. Imaging surface reactions with a photoemission electron microscope. *Journal Of Electron Spectroscopy and Related Phenomena* **98**, 41–54 (1999).
39. Michaelides, A. & Hu, P. Catalytic water formation on platinum: A first-principles study. *Journal of the American Chemical Society* **123**, 4235–4242 (2001).

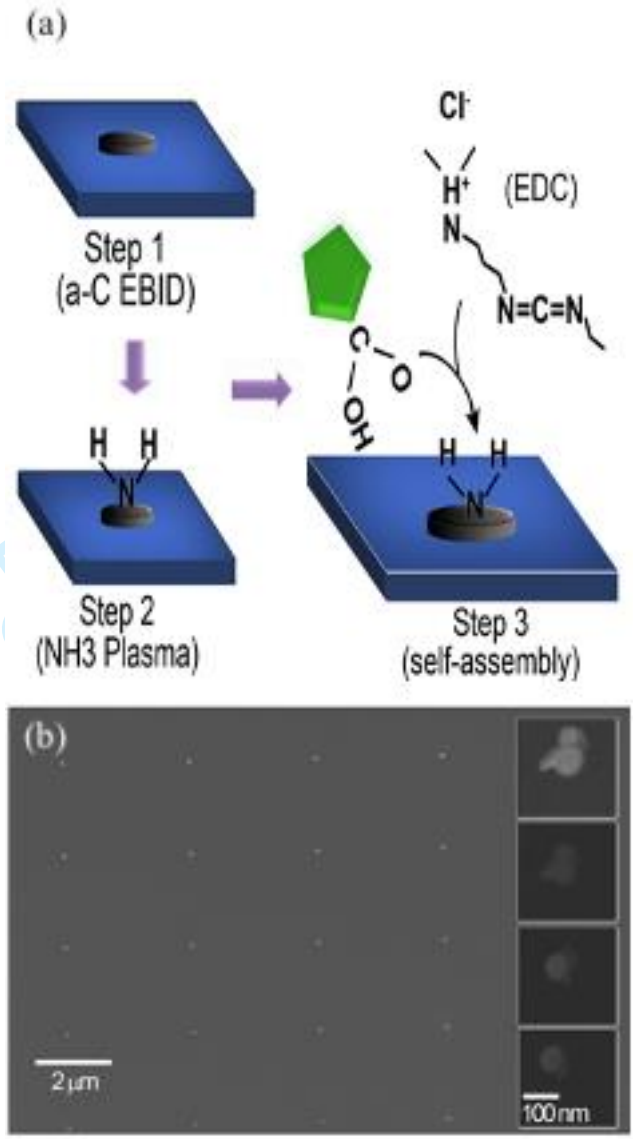

Fig. 1 – Nanodiamond beam-directed assembly process. (a) ESEM image of the electron beam deposited carbon seed array, and (b) steps involved in nanodiamond assembly on amine-functionalized carbon seeds. Insets in (b) are magnified images of four carbon seeds showing the successful attachment of nanodiamonds to each one.

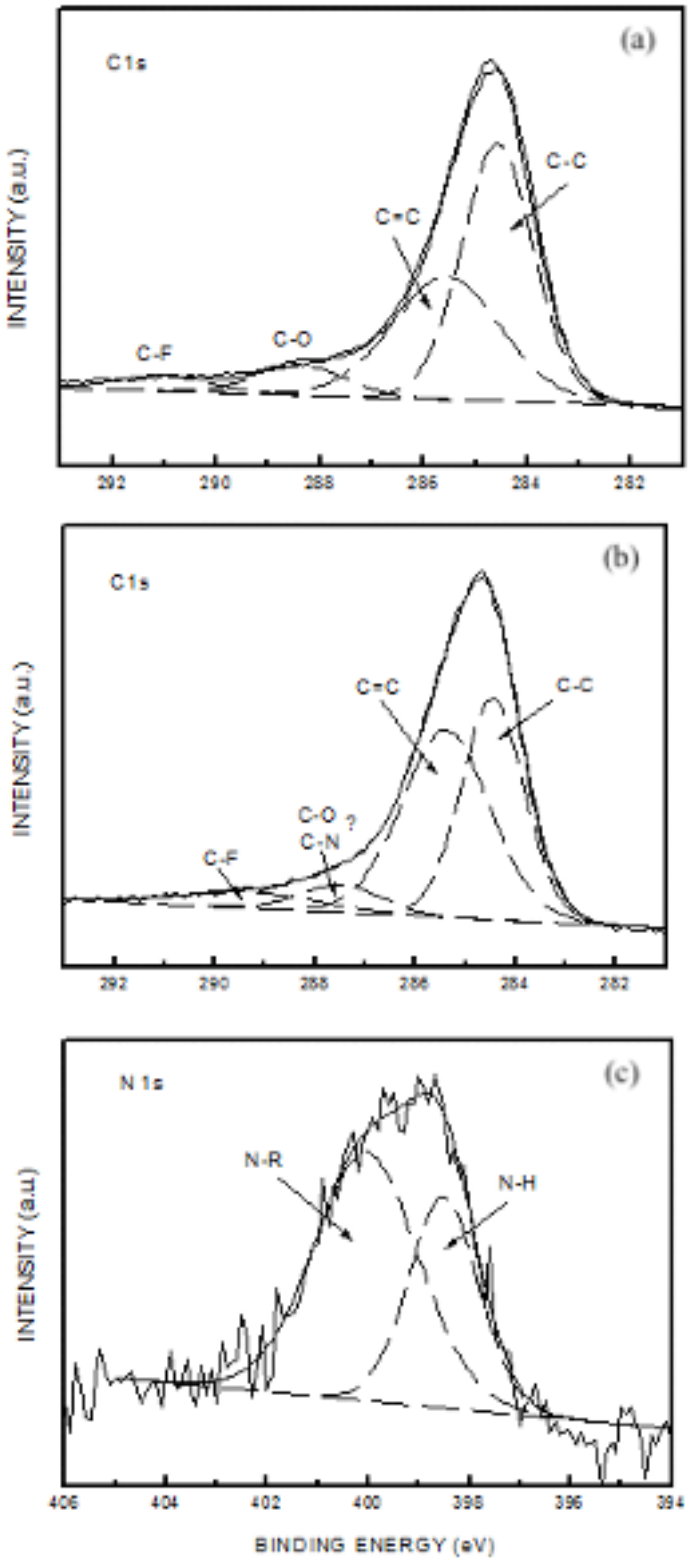

Fig. 2 – Surface modification of sputtered carbon with plasma treatment. (a) C 1s XPS spectrum of sputtered carbon film, (b) C 1s XPS spectrum of carbon film after ammonia plasma treatment, and (c) N 1s XPS spectrum of carbon film after ammonia plasma treatment.

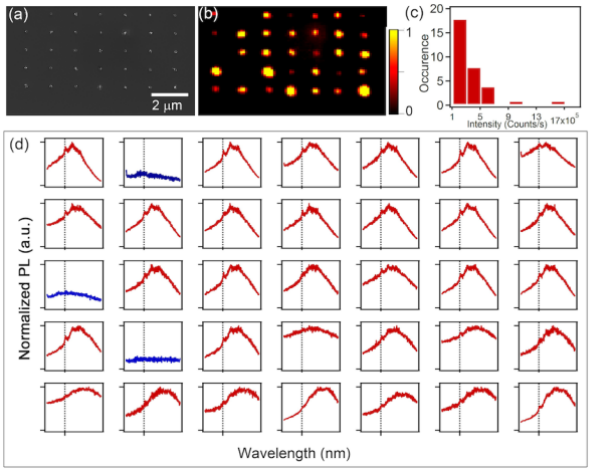

Fig. 3 – Optical characterization of nanodiamond attachment (reproduced from Fig. 2 of Ref. [21]). (a) SEM image of nanodiamond array, (b) Confocal PL of the same region, along with (c) histogram of the PL intensities, and (d) Normalized 637 nm PL emission from each spot in the array (red lines), where the position of the NV^- ZPL emission is marked by the dashed vertical line.

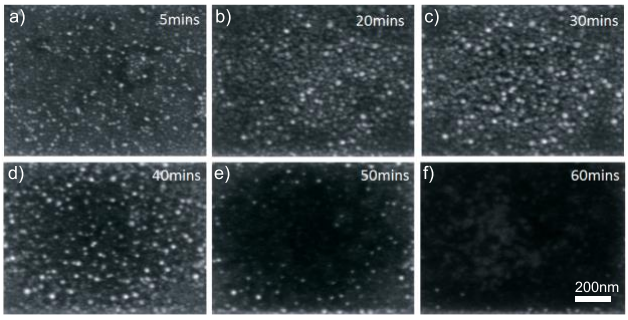

Fig. 4. Series of SEM images taken during H_2O-mediated electron beam induced etching of hBN, showing the initial formation of BN nanoparticles (a-c), followed by their eventual disappearance (d-f).

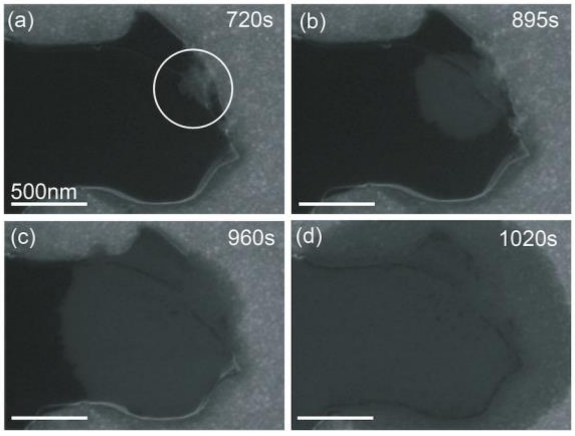

Figure 5. a-d) Series of ESEM micrographs showing the propagating reaction front resulting from the degradation of few-layered black phosphorus in H_2O at 25 C (RT) under electron irradiation at 15 keV and $4.42x10^{17}$ electrons $cm^{-2}min^{-1}$. In this case, the degradation reaction began at the centre of the circle marked in (a), at t_0=720 s.

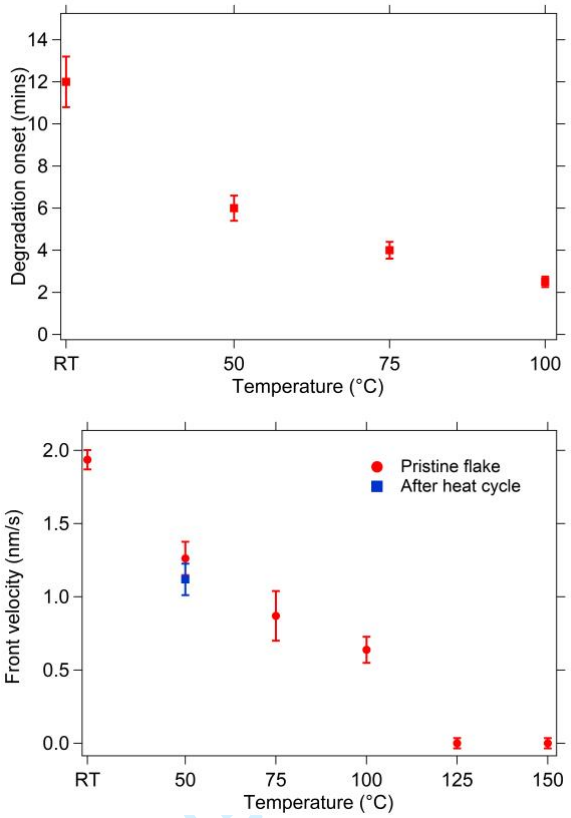

Figure 6. (a) Onset time for degradation (t_0, min.) at each temperature, and (b) front velocity of the reaction product formed by electron beam irradiation in H_2O at RT-150ºC. Measurements were conducted on a pristine BP flake (red), and on a heat-treated FLBP flake (blue) after a single heat cycle at 150ºC for 90 min.

Supplementary Material

Video taken during electron beam irradiation of BP in H_2O at 25ºC, from which the screen captures in Fig. 5 were taken.